# Emission of titanium dioxide nanoparticles from building materials to the environment by wear and weather

Neeraj Shandilya, Olivier Le Bihan, Christophe Bressot, Martin Morgeneyer

1  **Emission of Titanium Dioxide Nanoparticles from Building Materials to the**
2  **Environment by Wear and Weather**
3
4  *Neeraj Shandilya, Olivier Le Bihan, Christophe Bressot, Martin Morgeneyer\**
5
6  Neeraj Shandilya, Dr. Olivier Le Bihan, Dr. Christophe Bressot
7  Institut National de l'Environnement Industriel et des Risques (INERIS), Parc Technologique
8  Alata BP 2, 60550 Verneuil-en-Halatte, France
9
10  E-mail: martin.morgeneyer@utc.fr
11
12  Neeraj Shandilya, Dr.-Ing. Martin Morgeneyer
13  Université de Technologie de Compiègne (UTC), rue Roger Coutollenc, 60200 Compiègne,
14  France
15
16

17  **Abstract**

18  In the present work, we investigate the effect of the weathering duration on a commercial

19  photocatalytic nanocoating on the basis of its nanoparticles emission tendency into the two

20  media - air and water. It is found that the increase in the weathering duration results into the

21  stepwise structural deterioration of the nanocoating which, in turn, decreases the nanocoating

22  life, changes the nanocoating removal mechanism and increases the particle emission

23  concentration. The emission of the free $TiO_2$ nanoparticles is found to be weathering duration

24  dependent. Three quantities- Emission Transition Pace (ETP), Stable Emission Level (SEL)

25  and Stable Emission Duration (SED) are introduced. By linearly extrapolating these quantities

26  from short weathering durations, the complete failure of the nanocoatings can be predicted

27  and moreover the potential increase of nanoparticles release into the air.

28  **Keywords**: Weathering, Emission, Nanocoating

29

30  **Abstract Art**

31

32

33

## 1. Introduction

Photocatalytic nanocoatings are readily being applied on the external walls of buildings for their anti bacterial and self cleaning properties.[1, 2] These properties are ensured by the presence of embedded manufactured photocatalytic titanium dioxide ($TiO_2$) nanoparticles in the coating matrix. Resting on the external surfaces, these nanocoatings are frequently subjected to various mechanical solicitations and environmental weathering in real life conditions. [3, 4, 5] As a result, the consequent loss in their structural integrity leads to their disintegration which, in turn, may lead to the exposure of embedded nanoparticles [6] and thus their possible release too. Depending upon the type of medium in contact, this release can be into air as well as into ground waters. For a durable development, understanding their ecological and human health effects is important. In the last decade, slowly though, this concern has started gaining attention.[6-19] In this context, various toxicological and ecotoxicological studies have also demonstrated toxic effects of some types of $TiO_2$ nanoparticles.[20-25]

Here, the nanoparticles release from a commercial photocatalytic nanocoating is evaluated as a function of the duration of its weathering. Whilst the nanoparticles emission into air is studied via abrasion tests, their emission into water is studied via the microscopy and leaching tests of runoff samples. Through microscopic studies of the intermediate degraded states of the coated surfaces, the particles emission is shown to be weathering duration dependent.


## 2. Materials and Methods

### 2.1. Samples

For the study, a commercially available photocatalytic nanocoating, PHOTOCAL MASONRY, was chosen. It is manufactured by NANOFRANCE Technologies, France. It consists of anatase titanium dioxide nanoparticles having a primary size of <8 nm and a

2

59  volume percentage of 1.1%. Other material properties are as follows- Coagulation Index: ~2;

60  Appearance: white; Dispersant: Polymethylmethacrylate (PMMA). This type of nanocoating

61  is fabricated specifically for the applications on porous surfaces like brick, concrete etc. The

62  substrate chosen for the nanocoating application was a masonry brick (11 cm x 5 cm x 5 cm;

63  Leopard brick, Ref: 901796, Castorama, France). It is basically an alumino-silicate brick

64  which is frequently used in constructing façades, house walls, stairs etc. The microscopic

65  analysis of the nanocoating and the substrate were carried out using Optical Microscope

66  (Model Imager.M1m; Carl Zeiss MicroImaging GmbH; Germany), Energy Dispersion

67  Spectroscopy (EDS; Model X-max; Oxford Instruments UK) and Transmission Electron

68  Microscope (TEM; Model CM12; Philips, The Netherlands). Information on the microscopic

69  analysis results are provided in the separately available *supplementary part* of this paper. Four

70  coating layers with a total thickness of 80 µm approx. were applied on the brick substrates.

71  The substrate surfaces were prepared and the nanocoating was applied following the

72  guidelines in the technical data sheet recommended by the nanocoating manufacturer (i.e.

73  degreased using brush and ethanol soaked paper, dry and dust free surfaces; use of a High

74  Volume Low Pressure spray during coating; 25°C of ambient temperature).

75

76  **2.2. Artificial weathering**

77  The artificial weathering tests were performed with the nanocoated and the uncoated

78  reference brick samples in a weathering chamber (Model Suntest XLS+; Atlas; Germany).

79  The artificial weathering consisted of maximum 2658 cycles (which corresponds to 7 months)

80  of 2 hours each (120 min of UV light, 102 min dry, 18 min water spray). A xenon arc lamp

81  (300–400 nm; 60 W/m$^2$; Model NXE 1700; Ametek SAS; France) with an optical radiation

82  filter was used as the UV source. Such a system is a representative of natural sunlight.[20] The

83  temperature during UV exposure was monitored and averaged at 38 °C. The conditions were

84　chosen on the basis of an international standard.[26] De-ionized and purified water

85　(conductivity < 1 μS/cm) was used for the water spray onto the nanocoated samples. The

86　runoff water was collected in a reservoir, mounted at the bottom of the climate chamber. The

87　whole weathering process was intervened at selected times (2, 4, 6 and 7 months) for

88　analyzing the in-process condition of the test samples and sampling the collected runoff water

89　for its leaching analysis.

90

91　**2.3. Leaching**

92　To quantify the $TiO_2$ content in the leachate water, fixed amounts of samples (100 ml) were

93　collected at selected times (as indicated earlier) and analyzed by using Inductively Coupled

94　Plasma Mass Spectrometry (ICP-MS; Model 7500cx; Agilent Technologies; USA). The

95　operating conditions of the ICP-MS were as follows- Sample volume: 2 ml; RF Power: 1550

96　W; RF Matching: 1.78 V; Carrier Gas: 0.85 l/min; Makeup gas: 0.2 l/min; Nebulizer:

97　Micromist; Nebulizer pump: 0.1 r/s; S/C temperature: 15 °C; He flow rate: 5 ml/min; $H_2$ flow

98　rate: 2 ml/min; Integration time: 0.1 s; Chamber & Torch: Quartz; Cone: Ni; Element

99　detection threshold limit: 0.5 μg/l.

100

101　**2.4. Abrasion**

102　A modified Taber[TM] linear abrasion apparatus (Model 5750; Taber Inc. USA) [27] was used for

103　the abrasion of the nanocoated samples. The standard form of this apparatus is referenced in

104　numerous internationally recognized test standards.[28-30] This apparatus is already being used

105　in industries for analyzing the performance of products like paint, coating, metal, paper,

106　textile etc., during the application of a mechanical stress.[31] The normal stress of the abradant

107　of about 15 – 500 kPa, being applied through Taber, also corresponds to the typical normal-

108　and thus tangential- stress levels applied to surface coatings in a domestic setting, e.g. walking

109    with shoes, displacement of different furnishings etc.[3, 32] It incorporates a motor driven

110    horizontal arm (bar) that displaces an abradant in a back and forth linear motion over the test

111    sample. The abrasion is caused by the friction at the contact surface between the surfaces of

112    the abradant and the sample. Via a vertical shaft, a known weight is mounted on the top of the

113    abradant which shall be referred to as the *Normal Load* in the following text. The Taber[TM]

114    H38 non-resilient vitrified clay-carborundum abradant was used during the abrasion of the

115    nanocoated samples. This abradant comes in a cylindrical shape (6 mm diameter, 2 cm length)

116    and comprises of very fine abrasive particles (~4 µm) of carborundum that provide mild

117    abrasion. For reproducing the domestic stress conditions, a normal load of 6 N was chosen.

118    An abrasion stroke length of 76 mm, abrasion speed of 60 cycles/min and abrasion duration of

119    10 min were other selected parameters.

120

121    **2.5. Experimental set-up**

122    Figure 1 shows the scheme of the complete experimental set-up. Particle free air is passed

123    through a nanosecured work post (HPPE 10, Erma Flux S.A., France) containing the Taber

124    abrasion apparatus. Already been successfully employed in various nanoparticles' dustiness

125    tests,[33] this work post has a particle filter efficiency of 99.99%. The air flow rate inside this

126    work post is equal to 31000 l/min. The test sample is placed inside a self designed *Emission*

127    *Test Chamber* (0.5 m x 0.3 m x 0.6 m).[34] A small fraction of the air circulating inside the

128    nanosecured work post passes through the emission test chamber before starting the abrasion

129    tests in order to make it free from background particles. As soon as the chamber becomes

130    particle free, it is sealed completely. A slot is also provided on one of the walls of this

131    chamber allowing the horizontal arm of the abrasion apparatus passing through and operating

132    the motor unit placed externally. A radial symmetric sampling hood with a volume of 713 $cm^3$

133    provides an encapsulation of the sampling suction zone around the abradant. Such sampling

5

134   hood has also been employed in other studies with varying volumes, such as 1500 cm$^3$ by

135   Vorbau et al.[3] and 60 cm$^3$ by Gohler et al.[35]. Its use minimizes particle loss to the emission

136   test chamber's walls or other surfaces. Furthermore, the aerosol concentration remains

137   relatively high due to the low volume of the sampling hood and the fixed total sample flow

138   that amounts to 6.8 l/min. The Taber apparatus along with the emission test chamber

139   constitute the Aerosol Generation Section (*AGS*). The *AGS* is connected to an Aerosol

140   Measurement Section (*AMS*) using anti-static electrically conductive tubes (6 mm diameter)

141   where the generated aerosol particles are characterized in terms of their number concentration

142   and size distribution. The particle number concentration (*PNC*) can be defined as the number

143   of particles present in a unit centimeter cube of air at a given instant of time. The particle size

144   distribution (*PSD*) is the classification of the PNC according to their size. The instruments

145   used to measure these two quantities were: Condensation Particle Counter (CPC), Scanning

146   Mobility Particle Sizer (SMPS), Aerodynamic Particle Sizer (APS) and a Mini Particle

147   Sampler (MPS®; Ecomesure Inc. France).[36] The details on these instruments and their

148   operation conditions are shown in figure 1. Whilst the CPC measures the emitted aerosol

149   particles number concentration (EAPNC), the PSD is measured using SMPS and APS. A

150   MPS is used for the particle collection through filtration technique on copper mesh grids

151   which can be used later in TEM for various qualitative analyses of the emitted aerosol

152   particles without any limitation on the aerosol size. Therefore, the whole aerosol measurement

153   section, quantifying the particle emission, can measure aerosol particles having sizes ranging

154   from 4 nm to 20 µm.

155

156   **2.6. Background and particle loss**

157   Three empty test runs were done before the main abrasion experiment to measure the

158   concentration of the background particles and those generated by the motor in abrasion

159 apparatus. Without the test sample present in the chamber, the average concentration, detected

160 by CPC within the sampling hood, was ~ 0.7 $cm^{-3}$ with a standard deviation of 0.2 $cm^{-3}$.

161 Therefore, the concentrations of all the background particles and those generated by the

162 abrasion apparatus were insignificant. The calculations on the loss of particle concentration,

163 due to their deposition on the walls of the chamber, have shown a loss of 4% in number

164 during 10 min (i.e. the duration of the abrasion process).

165 For the present experimental set-up, the particle loss in the connecting tubes (i.e. losses due to

166 their gravitational settling, inertial deposition etc.) has been calculated by Shandilya et al. [37]

167 on the basis of system of equations enlisted by Brockmann et al. [38] Shandilya et al.[37] found it

168 to be 17% for particles having size less than or equal to 10 nm. For the 100 nm sized particles

169 or bigger, the loss reduces to mere 1%.

170

171 **3. Results and Discussion**

172 **3.1. Structural deterioration of nanocoated sample surfaces**

173 In figure 2 (a) to (e), the evolution in the surface deterioration of the nanocoated sample can

174 be observed with the increase in weathering duration. The optical microscopic image of a

175 non-weathered sample (figure 2 (a)) shows a continuous and intact form. With 2 months of

176 weathering (figure 2 (b)), *ridges* and *valleys* start to appear on the surface. If the weathering

177 continues, they develop into the cracks by 4 months of weathering (figure 2 (c)). After 6

178 months, these cracks start to broaden up with branching at different parts (figure 2 (d)). By 7

179 months, the nanocoating is no longer continuous but reduced in the form of *lumps* (figure 2

180 (e)). On the contrary, for an uncoated reference sample, no such effect of weathering was

181 observed throughout the whole process. In the literature, the cracking of water based

182 nanocoatings (as in present case) has been attributed mainly to two factors: drying stress due

183 to water content evaporation [39-42] and gradual embrittlement of the polymeric binder present

7

184    in the nanocoating during its interaction with UV rays.[43] Moreover, the cracking is often

185    accompanied by the shrinking or compaction of the nanocoating on the surface due to the

186    evaporation of the water content, as observed by Murray [40] and Dufresne et al. [41]

187    The nanocoating's shrinking and cracking may result in the exposure of the brick surface,

188    lying underneath. In order to confirm this hypothesis, EDS analysis of the weathered

189    nanocoated sample surfaces was done to create an elemental map between Ti (contributed by

190    the nancoating) and Ca (contributed by the brick). This would show the change in completely

191    exposed surfaces of the brick substrate. The results are shown in figure 2 (f) to (j). One may

192    see that while the Ti content on the surface remains approximately the same throughout the

193    weathering (average value ~16.1%), the Ca content and the exposed surface increase

194    proportionately. It directly implies the shrinkage of the nanocoating with weathering. If

195    continued further, the increased shrinking may even lead to the increase in Ti % density in the

196    nanocoating lumps.

197

198    **3.2. Particles emission into water by leaching**

199    For measuring the emission of $TiO_2$ nanoparticles in the water, 100 ml of leachate samples

200    were taken from the collected runoff water at selected times from a reservoir which was kept

201    beneath the nanocoated samples. For a detection threshold of 0.5 µg/l of an element, Ti was

202    found to be always below this threshold in the sample volume whereas the leached amount of

203    Ca (contributed by the brick) was found to be proportionally increasing with the weathering

204    duration. The TEM and EDS analysis of various droplets from the leachate samples (test

205    methodology and results described in supplementary information) showed irregularly shaped

206    *microsized* particle agglomerates.

207    In coherence with the ICP-MS measurements, the EDS analysis of these particle agglomerates

208    also showed an overall increasing Ca content, from 3 to 17% (by mass), with weathering. A

209    meager Ti content (0.2-1%, by mass) was observed in all particle agglomerates. The C content

210    (from nanocoating copolymer) was found to be varying from 3 to 10 % by mass. The other

211    dominating elements were Si (~32%, by mass) and Al (~20%, by mass). An increased water

212    conductivity (from <1 to 13 µS/cm) was also observed in the leachate samples which is

213    supposed to be a consequence of the increased presence of Si, Al and Ca.

214    This concludes that despite the deterioration by weathering, the nanocoated sample surfaces

215    are still strong enough to resist the leaching of the constituent nanoparticles in the runoff

216    water. Infact, it is the brick that obviously leaches its constituents in the runoff water. These

217    results seem to be consistent with Al-Kattan et al. [10] which studied the release of Ti, from

218    paints containing $TiO_2$ nanoparticles, into runoff water under the effect of artificial

219    weathering. They showed a close to background release of Ti, indicating that $TiO_2$

220    nanoparticles are strongly bound in the paint.

221

222    **3.3. Particles emission into air by abrasion**

223    Both uncoated reference and nanocoated samples were abraded after they were exposed to

224    weathering with varying durations. In figure 3 (a) and (b), TEM images of the emitted aerosol

225    particles are shown which were sampled and collected on mesh grids during the first 2

226    minutes of abrasion of the 4 and 7 months weathered nanocoated samples, respectively, under

227    the same sampling conditions. More aerosol particles get deposited on the mesh grids when

228    the weathering duration is increased from 4 to 7 months. When zoomed, irregularly shaped

229    polydispersed aerosol particles with no specific evolution in the shape, over the variation of

230    the weathering duration, were observed. Most importantly, for 7 months weathered

231    nanocoated samples, the presence of a considerable amount of free nanoparticles of $TiO_2$ (Ti

232    mass > 90%) was observed (figure 3 (c) & (d)). Since this result is in contrary to the findings

233    of numerous studies [4, 31, 35, 44], it is of more particular interest as these studies show that a large

234    fraction of the emitted nanomaterial is present in the matrix-bound form and not in the free

235    state. The increase in the relative % density of Ti, during the shrinking of the nanocoating

236    with the weathering, (as hypothesized earlier) may lead to the generation of these free $TiO_2$

237    nanoparticles.

238    The results on the chemical composition of the aerosol particles, generated from the abrasion

239    of 4 and 7 months weathered nanocoated samples, are shown in figure 3 (e). In this figure, the

240    average mass percentages of 3 elements- C (essentially coming from the nanocoating's

241    copolymer), Ti (essentially coming from the nanocoating) and Ca (essentially coming from

242    the brick)- are shown. One can observe a sharp drop in the relative C content (from 56% to

243    12%) while a sharp rise in the relative Ti content (from 7% to 55%) when the weathering

244    duration increases from 4 months to 7 months. Also, the relative Ca content, which is absent

245    in the case of 4 months weathered nanocoated samples, starts appearing and attains a value of

246    6% with 7 months of weathering. Hence, a direct impact of the weathering duration on the

247    size and chemical composition of the aerosol particles can be observed from these results.

248    Moreover, the chances of the exposure of free $TiO_2$ nanoparticles are much higher in the case

249    of 7 months weathered nanocoated samples.

250    The results on the EAPNC and PSD, measured within the volume of the sampling hood, are

251    shown in figure 4. In figure 4 (a) and (b), the abrasion test starts at t=120 s and ends at t= 720

252    s. Before and after this time interval (i.e. t=0 to 120 s and t=720 to 840 s), the abrasion

253    apparatus is at rest. For the uncoated reference samples, a constant EAPNC (~500 $cm^{-3}$; std.

254    deviation: 5 to 16 $cm^{-3}$; repeated thrice) is observed, regardless the weathering durations.

255    Hence, the artificial weathering has no apparent effect on the emitted aerosol particles from

256    the uncoated reference sample. However, for the nanocoated samples, the EAPNC increases

257    with the weathering duration. Except for 6 and 7 months, the nature of its variation with time

10

258    is also strikingly similar i.e. ascends initially, becomes constant, ascends again and becomes

259    constant at last (the PSD, during the first constant phase, is shown in figure 4(d)).

260    For 6 and 7 months weathered nanocoated samples, we observe a rise in the EAPNC curves

261    during their initial phases (t= 120 s to t= 360 s) beyond the maximum level observed for the

262    shorter weathering durations. After t= 360 s, these curves tend back to the same level as that

263    of the uncoated reference and their counterparts. Such a behavior can be explained on the

264    basis of the nanocoating removal mechanism during the abrasion of the weathered nanocoated

265    samples. In case of non-weathered, 2 and 4 months weathered nanocoated samples, the

266    dominant material removal mechanism is assumed to be *abrasion wear* of the nanocoating

267    due to its continuous and stable form. But for 6 and 7 months weathered nanocoated samples,

268    it is hypothesized that the dominant material removal is rather *uprooting* of the nanocoating

269    lumps (or soon to be lumps) by the abradant. Since these lumps are loosely attached to the

270    surface, their uprooting is faster and easier. As a result, the EAPNC reaches its highest level

271    as soon as the abrasion starts and comes back to the same level, later, as that of the uncoated

272    reference, when all the nanocoating lumps have been uprooted and the brick surface is

273    completely exposed.   The PSD, shown in figure 4 (c) and (d) for uncoated reference and

274    nanocoated samples respectively, vary in a different manner with respect to each other. Whilst

275    for the uncoated reference samples, there is no significant change in the size mode (alternating

276    between 250 nm to 350 nm) and maximum PNC (lying around 375 cm$^{-3}$, std. dev.: 0.2 to 8

277    cm$^{-3}$), a continuous evolution can be observed in these two parameters in case of the

278    nanocoated samples.

279    Coming back to the nature of the EAPNC variation with time, as observed in figure 4 (b), an

280    analytic model had been presented by Shandilya et al. [46] which approximates such a variation

281    in terms of 4 phases for the present nanocoating and one other commercial one: Tipe® E502,

282    TitanPE Technologies, Inc. (see figure 5). When an uncoated reference sample is abraded

11

283 (figure 4 (a)), the EAPNC reaches a maximum limit swiftly (represented by segment **EF** in

284 figure 5(a); named as *phase I*) and then remains constant until the end of the abrasion

285 (represented by segment **FI** in figure 5(a); named as *phase IV*). However, the EAPNC, in case

286 of a nanocoated sample (figure 4 (b)), passes through two intermediate phases (represented by

287 segments **FG** & **GH** in figure 5(b); named as *phases II* and *III* resp.) before becoming

288 constant at the end i.e. *phase IV*. Obviously, for an uncoated surface, the phases II and III are

289 absent in the evolution of the EAPNC.

290 If physically interpreted, the *phase I* is contributed by the evolution of the contact surface

291 conditions between the abradant and the nanocoated sample surface when the abrasion starts.

292 During this phase, an ascending EAPNC is observed. In *phase II*, the EAPNC is constant and

293 the abrasion of the nanocoated sample surface takes place under a stable state. The

294 nanocoating is getting removed gradually or slowly through its abrasion wear. The duration of

295 this phase also signifies the apparent nanocoating life. By the end of *phase II*, the surface

296 nanocoating layer is no more stable and just the nanocoating-brick interface is left. With the

297 advent of *phase III*, the brick surface starts to get exposed gradually and by the end of this

298 phase, it is completely exposed. Therefore, the EAPNC, during *phase IV*, arrives at the same

299 level as that of an uncoated reference sample and remains constant afterwards.

300 Three quantities:

301 (i) **Emission Transition Pace (ETP)** i.e. $(\Delta C/\Delta t)_I$ ;

302 (ii) **Stable Emission Level (SEL)** i.e. $(\#C)_{II}$;

303 (iii) **Stable Emission Duration (SED)** i.e. $T_{II}$

304 can also be identified from figure 5 (a) and (b) and are discussed in the following. These are

305 the important indicators for assessing the nanocoating useful life and EAPNC. In figure 6 (a)

306 and (b), they are plotted as a function of the weathering duration. In figure 6 (a), we see that

307 the **ETP** (defined as the rate of change of the EAPNC) increases with weathering duration for

308   weathered nanocoated samples whereas for the uncoated reference, it remains constant.

309   Moreover, *ETP* values for non-weathered, 2 and 4 months weathered nanocoated samples lie

310   beneath the uncoated reference sample. But for 6 and 7 months weathered nanocoated

311   samples, they lie above. On the basis of figure 2 and 4, we have already hypothesized a

312   change in the nanocoating removal mechanism during the transition of the weathering

313   duration from 4 to 6 months. Therefore, one may conclude that if the *ETP* value of the

314   EAPNC, from a nanocoated sample, lies beneath the one corresponding to its uncoated

315   reference substrate, the nanocoating removal mechanism is dominated by the abrasion wear.

316   If opposite, the uprooting of the nanocoating is more dominant. Under given abrasion

317   conditions, if *ETP* does not increase with the weathering duration (as observed in case of the

318   uncoated reference), it implies no change in the abrasion conditions, regardless of the

319   weathering duration. But if it increases (as observed in case of the weathered nanocoated

320   samples), it implies the change in the abrasion conditions. In the present case, such a change

321   is imparted by the deterioration of the nanocoating, as shown, qualitatively, in figure 2. The

322   second quantity, **SED**, is a direct indicator of the nanocoating life - higher the *SED*, higher is

323   the nanocoating life time. It appears to decrease with the weathering duration (figure 6 (b)).

324   When SED= 0, it means that the nanocoating disappears as soon as its abrasion starts.

325   Quantitatively, it allows extrapolating the effect of the shorter weathering durations to that of

326   the longer ones without prolonging the weathering test in reality. In figure 6 (b), if the SED

327   average values, from first 2 months of weathering, are extrapolated, we observe that SED

328   reduces to 0 in 11 months. The extrapolation of the extreme limits (i.e. through maximum

329   value of SED for 0 months and minimum value of SED for 2 months) can be used to calculate

330   the minimum useful life of the nanocoating under present weathering conditions. If it is done

331   in the present case, we observe that SED reduces to 0 in 6 months- this is exactly what we

332   observe in the figure 6 (b). Moreover, the average value of *SED* is decreasing from 320 s to

13

333    110 s (i.e. a reduction factor of ~3) in mere first 4 months of weathering. The EAPNC during

334    SED is equal to **SEL**. In figure 6 (b), it appears to increase with the weathering duration.

335    Since SED= 0 for 6 and 7 months of weathering, therefore, SEL value for these durations

336    cannot be calculated.

337    If summarized, we can say that under the present experimental conditions, a step-wise and

338    complete surface deterioration of the nanocoated samples was observed as a function of the

339    duration of a weathering by UV, temperature and water. This surface deterioration led directly

340    to an increase of the emitted aerosol particles number concentration (measured within the

341    volume of the sampling hood) and the $TiO_2$ content of the aerosolized wear particles. A

342    considerable presence of free $TiO_2$ nanoparticles was observed in the case of the 7 months

343    weathered nanocoated samples. This was a fundamental change observed in the chemical

344    composition of the aerosol particles, as for short weathering durations, $TiO_2$ nanoparticles

345    were always found to be embedded inside the released coarse wear particles with a polymeric

346    matrix. This increase might still continue for longer weathering durations. With a high

347    specific surface area, these free nanoparticles aerosols now accentuate a potential risk in terms

348    of nano- toxicity. In case of leaching, no such effects were observed during 7 months of

349    weathering. However, fears still remain on how and in what concentrations the leaching of

350    $TiO_2$ might occur during prolonged weathering durations. This study also proposed an outline

351    to understand the phenomenon of aerosolization and the indicators, like *Emission Transition*

352    *Pace*, *Stable Emission Level* and *Stable Emission Duration*, for its monitoring. They were

353    found to be significant to quantitatively predict the emitted aerosol particles number

354    concentration and nanocoating useful life by the means of linear extrapolation from shorter

355    weathering durations. It is possible to extend this study to a broad spectrum of nanocoatings,

356    with the prospect of seeking their optimal formulations on the basis of nano risk i.e. emissions

357    control.

14

**Supporting Information Available**

 More details on the materials used during the study can be found in the supporting information. This information is available free of charge via the Internet at http://pubs.acs.org/.

**Acknowledgements**

[1] Torgal, F.P.; Jalali, S. Eco-efficient construction and building materials. *Constr. Build. Mater.* **2011**, *25*, 582-590.

[2] Stamate, M.; Lazar, G. Application of titanium dioxide photocatalysis to create self-cleaning materials. *Romanian Technical Sciences Academy MOCM* **2007**, 13-3, 280-285.

[3] Vorbau, M.; Hillemann, L.; Stintz, M. Method for the characterization of the abrasion induced nanoparticle release into air from surface coatings. *Aerosol Sci* **2009**, 40, 209-217.
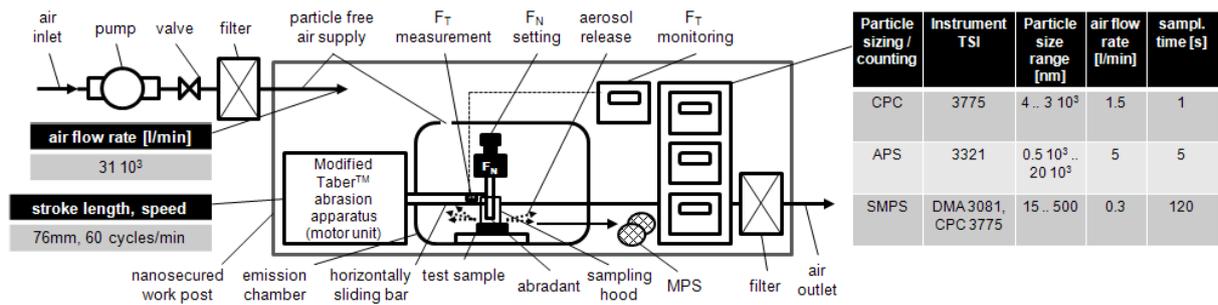
382   [4]   Shandilya, N.; Le Bihan, O.; Morgeneyer, M. A review on the study of the generation of

383         (nano-) particles aerosols during the mechanical solicitation of materials. *J Nanomater*

384         **2014**, Art. ID 289108.

385   [5]   Le Bihan, O.; Shandilya, N.; Gheerardyn, L.; Guillon, O.; Dore, E.; Morgeneyer, M..

386         Investigation of the Release of Particles from a Nanocoated Product. *Advances in*

387         *Nanoparticles* **2013**, 2, 39-44.

388   [6]   Göhler, D.; Nogowski, A.; Fiala, P.; Stintz, M. Nanoparticle release from nanocomposites

389         due to mechanical treatment at two stages of the life-cycle. *J Phys Conf Ser* **2013** 429

390         (2013) 012045; DOI: 10.1088/1742-6596/429/1/012045.

391   [7]   Allen, N.S.; Edge, M.; Corrales, T.; Childs, A.; Liauw, C.M.; Catalina, F.; Peinado, C.;

392         Minihan, A.; Aldcroft, D. Ageing and stabilisation of filled polymers: an overview.

393         *Polym Degrad Stabil* **1998**, 61, 183-199.

394   [8]   Allen, N.S.; Edge, M.; Ortega, A.; Sandoval, G.; Liauw, C.M.; Verran, J.; Stratton, J.;

395         McIntyre, R.B. Degradation and stabilisation of polymers and coatings: nano versus

396         pigmentary titania particles. *Polym Degrad Stabil* **2004**, 85, 927-946.

397   [9]   Hsu, L.Y.; Chein, H.M. Evaluation of nanoparticle emission for $TiO_2$ nanopowder

398         coating materials. *J Nanopart Res* **2007**, 9, 157-163.

399   [10] Al-Kattan, A.; Wichser, A.; Vonbank, R.; Brunner, S.; Ulrich, A.; Zuind, S.; Nowack, B.

400         Release of $TiO_2$ from paints containing pigment-$TiO_2$ or nano-$TiO_2$ by weathering. *Env*

401         *Sci Process Impact* **2013**, 15, 2186-2193.

402   [11] Kaegi, R.; Ulrich, A.; Sinnet, B.; Vonbank, R.; Wichser, A.; Zuleeg, S.; Simmler, H.;

403         Brunner, S.; Vonmont, H.; Burkhardt, M.; Boller, M. Synthetic $TiO_2$ nanoparticle

404         emission from exterior facades into the aquatic environment. *Environ Pollut* **2008**, 156,

405         233-239.

406 [12] Hirth, S.; Cena, L.; Cox, G.; Tomovic, Z.; Peters, T.; Wohlleben, W. Scenarios and

407 methods that induce protruding or released CNTs after degradation of nanocomposite

408 materials. *J Nanopart Res* **2013**, 15, 1504-1518.

409 [13] Wohlleben, W.; Brill, S.; Meier, M. W.; Mertler, M.; Cox, G.; Hirth, S.; von Vacano, B.;

410 Strauss, V.; Treumann, S.; Wiench, K.; Ma-Hock, L.; Landsiedel, R. On the lifecycle of

411 nanocomposites: comparing released fragments and their in vivo hazards from three

412 release mechanisms and four nanocomposites. *Small* **2011**, 7, 2384-2395.

413 [14] Al-Kattan, A.; Wichser, A.; Zuin, S.; Arroyo, Y.; Golanski, L.; Ulrich, A.; Nowack, B.

414 Behavior of TiO2 released from nano-TiO2-containing paint and comparison to pristine

415 nano-TiO$_2$. *Environmental Science & Technology* **2014**, 48, 6710-6718.

416 [15] Gondikas, A. P.; von der Kammer, F.; Reed, R. B.; Wagner, S.; Ranville, J. F.; Hofmann,

417 T. Release of TiO$_2$ nanoparticles from sunscreens into surface waters: a one-year survey

418 at the old danube recreational lake. *Environmental Science & Technology* **2014**, 48, 5415-

419 5422.

420 [16] von Goetz, N.; Lorenz, C.; Windler, L.; Nowack, B.; Heuberger, M.; Hungerbuhler, K.

421 Migration of Ag- and TiO$_2$- (nano)particles from textiles into artificial sweat under

422 physical stress: experiments and exposure modeling. *Environmental Science &*

423 *Technology* **2013**, 47, 9979-9987.

424 [17] Windler, L.; Lorenz, C.; von Goetz, N.; Hungerbuhler, K.; Amberg, M.; Heuberger, M.;

425 Nowack, B. Release of titanium dioxide from textiles during washing. *Environmental*

426 *Science & Technology* **2012**, 46, 8181-8188.

427 [18] Zhang, W.; Crittenden, J.; Li, K. G.; Chen, Y. S.; Attachment efficiency of nanoparticle

428 aggregation in aqueous dispersions: modeling and experimental validation.

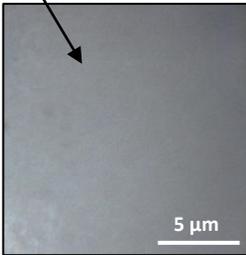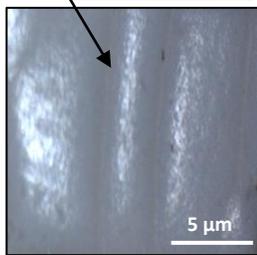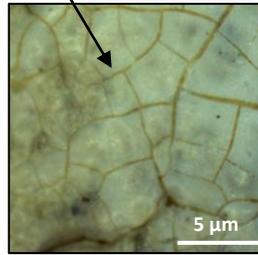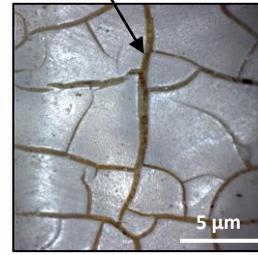429 *Environmental Science & Technology* **2012**, 46, 7054-7062.

430    [19] Stefano, Z.; Marco, G.; Arlen, F.; Luan, G. Leaching of nanoparticles from experimental
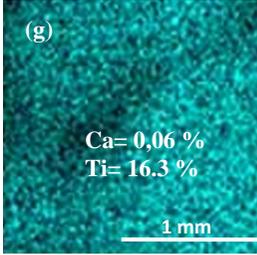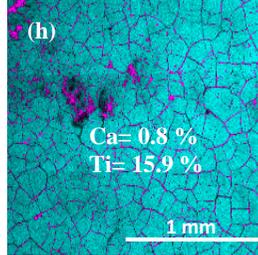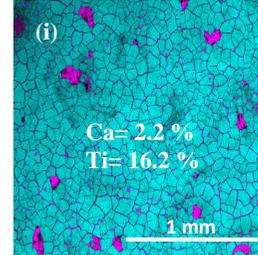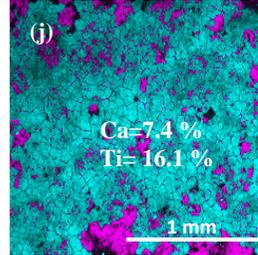
431         water-borne paints under laboratory test conditions. *Journal of Nanoparticle Research*

432         **2013**, 16, 2185.

433    [20] Petkovic, J.; Zegura, B.; Stevanovic, M.; Drnovsek, N.; Uskokovic, D.; Novak, S. DNA

434         damage and alterations in expression of DNA damage responsive genes induced by $TiO_2$

435         nanoparticles in human hepatoma HepG2 cells. *Nanotoxicology* **2011**, 5, 341-353.

436    [21] Unnithan, J.; Rehman, M.U.; Ahmad, F.J.; Samim, M. Aqueous Synthesis and

437         Concentration-Dependent dermal toxicity of $TiO_2$ nanoparticles in wistar rats. *Biol Trace*

438         *Elem Res* **2011**, 143, 1682-1694.

439    [22] Warheit, D.B.; Brock, W.J.; Lee, K.P.; Webb, T.R.; Reed, K.L. Comparative pulmonary

440         toxicity inhalation and instillation studies with different $TiO_2$ particle formulations.

441         *Toxicol Sci* **2005**, 88, 514-524.

442    [23] Yamashita, K.; Yoshioka, Y.; Higashisaka, K.; Mimura, K.; Morishita, Y.; Nozaki, M.;

443         Yoshida,  T.; Ogura, T.; Nabeshi, H.; Nagano, K.; Abe, Y.; Kamada, H.; Monobe, Y.;

444         Imazawa, T.; Aoshima, H.; Shishido, K.; Kawai, Y.;   Mayumi, T.; Tsunoda, S.; Itoh, N.;

445         Yoshikawa, T.; Yanagihara, I.; Saito, S.; Tsutsumi, Y. Silica and titanium dioxide

446         nanoparticles cause pregnancy complications in mice. *Nat Nanotechnol* **2011**, 6, 321-328.

447    [24] Barnard, A.S. One-to-one comparison of sunscreen efficacy, aesthetics and potential

448         nanotoxicity.  *Nat Nanotechnol* **2010**, 5, 271-274.

449    [25] Auffan, M.; Rose, J.; Bottero, J.Y.; Lowry, G. V.; Jolivet, J.P.; Wiesner, M. R. Towards a

450         definition of inorganic nanoparticles from an environmental, health and safety

451         perspective.  *Nat Nanotechnol* **2009**, 4, 634-641.

452    [26] AFNOR. Paints and varnishes – Methods of exposure to laboratory light sources – Part 1:

453         General guidance, ISO 16474-1, **2012**.

454 [27] Morgeneyer, M.; Shandilya, N.; Chen, Y.M.; Le Bihan, O. Use of a modified Taber

455     abrasion apparatus for investigating the complete stress state during abrasion and in-

456     process wear particle aerosol generation. *Chem Eng Res Des*, DOI:

457     http://dx.doi.org/10.1016/j.cherd.2014.04.029

458 [28] ASTM. International. Standard Test method for the abrasion of organic coatings by the

459     Taber Abradant, ASTM D4060, **2007**.

460 [29] ASTM. International. Standard Test Methods for Dry Abrasion Mar Resistance of High

461     Gloss Coatings, ASTM D6037, **1996**.

462 [30] ASTM. International, Standard Test Method for Resistance of Transparent Plastics to

463     Surface Abrasion, ASTM D1044, **2008**.

464 [31] Golanski, L.; Guiot, A.; Pras, M.; Malarde, M.; Tardif, F. Release-ability of nano fillers

465     from different nanomaterials (toward the acceptability of nanoproduct). *J Nanopart Res*

466     **2012**, 14, 962-970.

467 [32] Hassan, M.M.; Dylla, H.; Mohammad, L.N.; Rupnow, T. Evaluation of the durability of

468     titanium dioxide photocatalyst coating for concrete pavement. *Constr Build Mater* **2010**,

469     24, 1456-1461.

470 [33] Morgeneyer, M.; Le Bihan, O.; Ustache, A.; Aguerre Chariol, O. Experimental study of

471     the aerosolization of fine alumina particles from bulk by a vortex shaker. *Powder Technol*

472     **2013**, 246, 583-589.

473 [34] Le Bihan, O.; Morgeneyer, M.; Shandilya, N.; Aguerre Chariol, O.; Bressot, C. In

474     *Handbook of Nanosafety- Measurement, Exposure and Toxicology*; Vogel, U.,

475     Savolainen, K., Wu, Q., Van Tongeren, M., Brouwer, D., Berges M., Eds.; Academic

476     Press: San Diego **2014**; Ch. 7

477 [35] Göhler, D.; Stintz, M.; Hillemann, L.; Vorbau, M. Characterization of Nanoparticle

478     Release from Surface Coatings by the Simulation of a Sanding Process. *Ann Occup Hyg*

479     **2010**, 54, 615-624.

480 [36] R'mili, B.; Le Bihan, O.; Dutouquet, C.; Aguerre Charriol, O.; Frejafon, E. Sampling by

481     TEM Grid Filtration. *Aerosol Sci Tech* **2013**, 47, 767-775.

482 [37] Shandilya, N.; Le Bihan, O.; Morgeneyer, M., Effect of the normal load on the release of

483     aerosol wear particles during abrasion. *Tribol Lett* **2014**, 55, 227-234.

484 [38] Brockmann, J.E. In *Aerosol Measurement- Principles, Techniques and Applications*;

485     Kulkarni, P., Baron, P.A., Willeke, K., Eds.; John Wiley & Sons: New Jersey **2011**, Ch.

486     6.

487 [39] White, L.R. Capillary rise in powders. *J Colloid Interf Sci* **1982**, 90, 536-538.

488 [40] Murray, M. Cracking in coatings from colloidal dispersions: An industrial perspective.

489     Proceedings Rideal Lecture, London, 20 April **2009**.

490 [41] Dufresne, E.R.; Corwin, E.I.; Greenblatt, N.A.; Ashmore, J.; Wang, D.Y.; Dinsmore,

491     A.D.; Cheng, J.X.; Xie, X.S.; Hutchinson, J.W.; Weitz, D.A. Flow and Fracture in Drying

492     Nanoparticle Suspensions.  *Phys Rev Lett* **2003**, 91, 224501-1 - 224501-4.

493 [42] Tirumkudulu, M.S.; Russel, W.B. Cracking in Drying Latex Films. *Langmuir* **2005**, 21,

494     4938-4948.

495 [43] Hare, C.H. The Degradation of Coatings by Ultraviolet Light and Electromagnetic

496     Radiation. *Protective Coatings and Linings* **1992**.

497 [44] Shandilya, N.; Le Bihan, O.; Bressot, C.; Morgeneyer, M. Evaluation of the particle

498     aerosolization from n-$TiO_2$ photocatalytic nanocoatings under abrasion. *J Nanomater*

499     **2014**, Art. ID 185080.

air inlet — pump — valve — filter — particle free air supply — $F_T$ measurement — $F_N$ setting — aerosol release — $F_T$ monitoring

**air flow rate [l/min]**
31 $10^3$

**stroke length, speed**
76mm, 60 cycles/min

Modified Taber™ abrasion apparatus (motor unit)

nanosecured work post — emission chamber — horizontally sliding bar — test sample — abradant — sampling hood — MPS — filter — air outlet

| Particle sizing / counting | Instrument TSI | Particle size range [nm] | air flow rate [l/min] | sampl. time [s] |
|---|---|---|---|---|
| CPC | 3775 | 4 .. 3 $10^3$ | 1.5 | 1 |
| APS | 3321 | 0.5 $10^3$ .. 20 $10^3$ | 5 | 5 |
| SMPS | DMA 3081, CPC 3775 | 15 .. 500 | 0.3 | 120 |

**Figure 1.** Experimental set-up

| | No weathering | 2 months of weathering | 4 months of weathering | 6 months of weathering | 7 months of weathering |
|---|---|---|---|---|---|
| Optical Microscopy of the nanocoated test samples | **(a)** Continuous and intact form of the nanocoating — 5 µm | **(b)** Ridge and valley formation on the nanocoated surface — 5 µm | **(c)** Cracking of the nanocoated surface — 5 µm | **(d)** Crack broadening — 5 µm | **(e)** Lump formation — 5 µm |
| Spatial distribution mapping of Ca and Ti over nanocoated test samples<br><br>Ca ▮<br>Ti ▮ | **(f)** Ca= 0 %<br>Ti= 16.2 %<br>1 mm<br>Nanocoating deposited all over the surface | **(g)** Ca= 0,06 %<br>Ti= 16.3 %<br>1 mm<br>No effect;<br>Exposed surface = 0.1 mm² | **(h)** Ca= 0.8 %<br>Ti= 15.9 %<br>1 mm<br>Brick exposure through cracks;<br>Exposed surface = 0.53 mm² | **(i)** Ca= 2.2 %<br>Ti= 16.2 %<br>1 mm<br>Exposed surface = 1.19 mm² | **(j)** Ca=7.4 %<br>Ti= 16.1 %<br>1 mm<br>Exposed surface = 2.83 mm² |
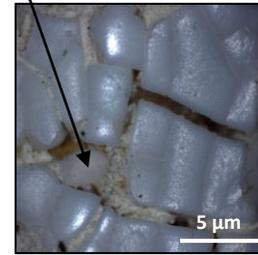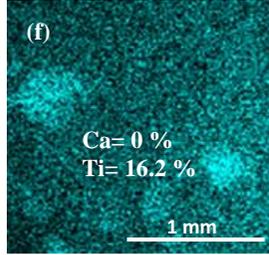
**Figure 2.** Microscopic analysis of the nanocoated sample
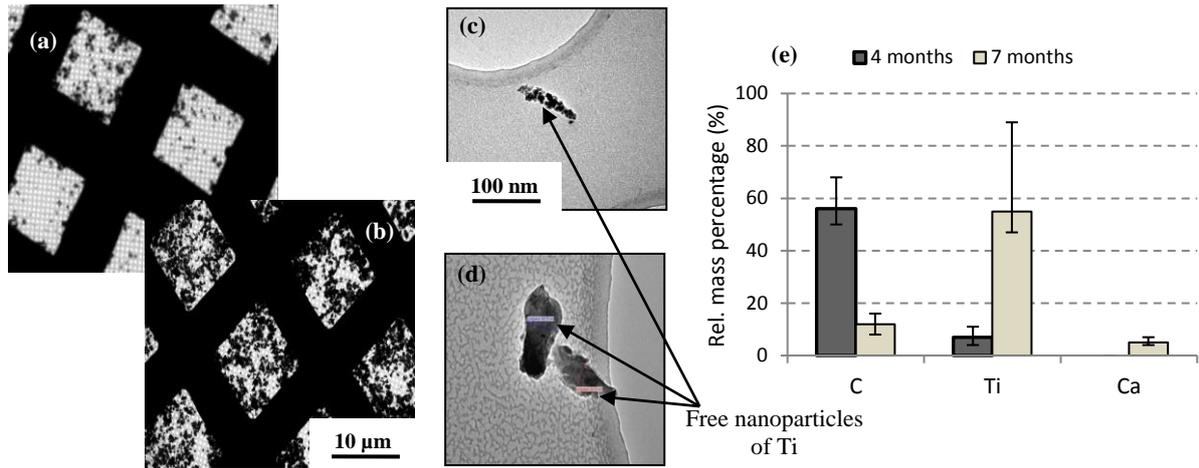
**Figure 3.** TEM image of the aerosol particles emitted from the abrasion of **(a)** 4 months **(b)** 7 months weathered nanocoated samples **(c), (d)** Free nanoparticles emitted from the abrasion of 7 months weathered nanocoated samples **(e)** Chemical analysis of the aerosol particles emitted from the abrasion of 4 and 7 months weathered nanocoated samples
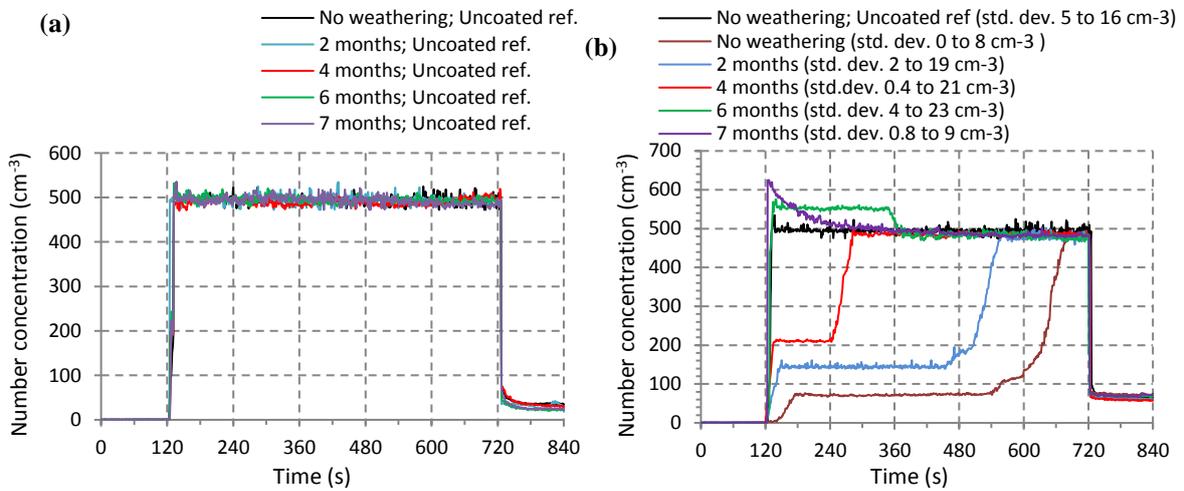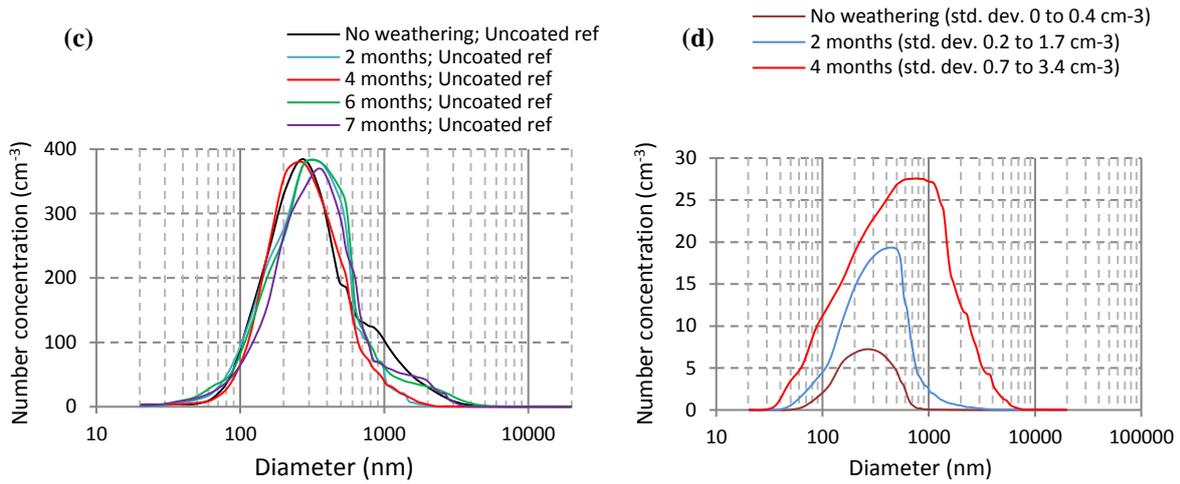
**Figure 4.** EAPNC during the abrasion of weathered **(a)** uncoated reference sample **(b)**

nanocoated samples

PSD of the emitted aerosol particles during the abrasion of weathered **(c)** uncoated reference

sample (t= 120 s to 720 s) **(d)** nanocoated samples (corresponding to the phase during which

the concentration is constant for the first time in figure 4 (b))
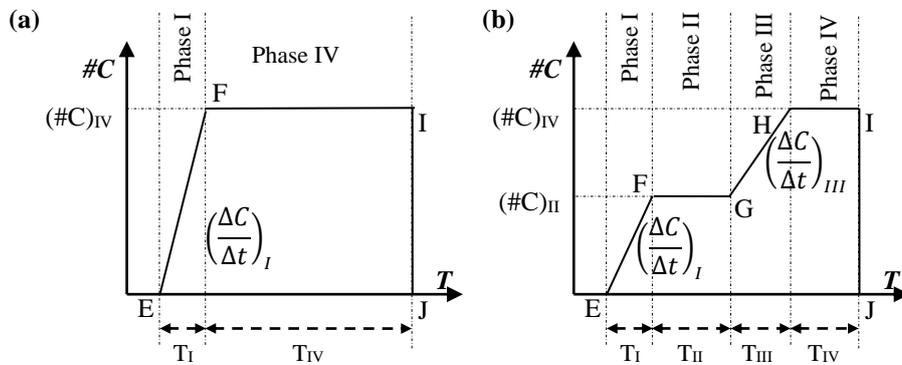


**Figure 5.** Variation of aerosol particle number concentration generated from **(a)** uncoated and

**(b)** nanocoated surface samples
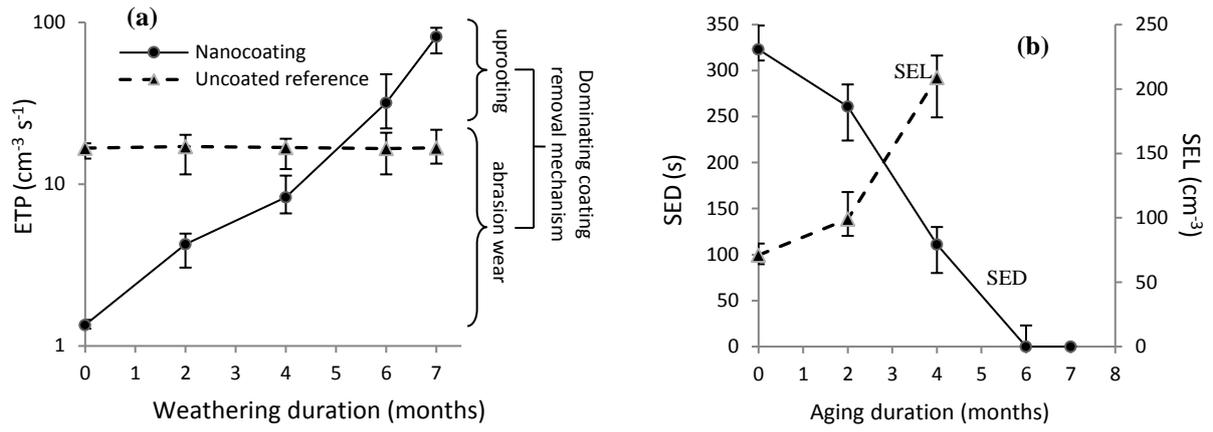
**Figure 6.** Variation of (**a**) ETP (**b**) SED and SEL with the weathering duration